Parametric identification of viscoelastic materials from time and frequency domain data*

M. Mossberg[†], L. Hillström[‡], and L. Abrahamsson[§]

April 17, 2000

Abstract

In this paper a parametric model of the elasticity modulus of a viscoelastic material (polypropylene) is determined by measured strains from wave propagation experiments. The identification of the model parameters is carried out both in the time and in the frequency domain. The advantages and limitations of either approach is discussed. Our main result is that a good representation of the elasticity modulus can be obtained by a general standard linear solid with three elements or seven free parameters. The model is valid over the same frequency range as that of the data, which in the present case extends from 100 Hz to 10 kHz. Such a model makes it possible to perform direct time simulations by time-stepping algorithms.

Keywords: viscoelastic, wave propagation, complex modulus, parametric, estimation, time domain, frequency domain, finite differences.

1 Introduction

Viscoelastic materials are used in a wide range of applications [12]. It is therefore important to fully characterise the properties of such materials. Material identification methods based on time-harmonic wave propagation is of particular importance in linear viscoelasticity. In the frequency domain the viscoelastic stress-strain relationship is identical to the purely elastic one except that the elastic moduli are complex valued. For one-dimensional viscoelastic wave propagation it implies that the solution, for homogeneous materials, can be written

*Work supported by Swedish Research Council for Engineering Sciences under contracts 96–212 and 98–137.

[†]Dept. of Systems and Control, Information Technology, Uppsala University, Box 27, SE-751 03 Uppsala, Sweden, E-mail: mm@syscon.uu.se

[‡]Ångström Laboratory, Uppsala University, Box 534, SE-751 21 Uppsala, Sweden, E-mail: lars.hillstrom@material.uu.se

[§]Dept. of Scientific Computing, Information Technology, Uppsala University, Box 120, SE-751 04 Uppsala, Sweden, E-mail: leif.abrahamsson@tdb.uu.se

as a sum of exponentials with wave numbers that depend solely on the frequency and the medium. This has been basic to the determination of complex moduli from measurements on longitudinal or torsional vibrations in excited rods [2, 15, 17, 24].

The objective of this work is to derive a parametric model of the viscoelastic behaviour that is useful for direct time domain simulations of wave propagation phenomena. Such a model must be causal and accurate over an appropriate frequency range corresponding to the spectral content of the source of excitation. In addition, it must be suitable for a numerical treatment by a time-stepping algorithm like the finite difference method. A direct numerical implementation of the most general linear constitutive stress-strain relationship as a convolution integral would be too cumbersome. Likewise a description of the viscoelastic modulus in the frequency domain in the form of a table or a graph is intractable in the time domain. This difficulty can be avoided by a differential description of rheology effects [3, 6, 7, 18]. This representation is equivalent to a mechanical model consisting of an array of standard linear solid elements connected in parallel [4]. In the frequency domain such a model is described by a rational transfer function between stress and strain. In the time domain it can be written as a system of ordinary differential equations of first order which is easy to incorporate into a finite difference method. There are essentially two free parameters (relaxation times) associated with each standard linear solid element. These parameters were estimated by the use of measured strains from wave propagation experiments. The optimal values were found by minimising the difference between the measured strains and those computed by the wave propagation model.

The main result of the paper is that a quite accurate representation of the elastic modulus of a specific material (polypropylene) could be obtained by a general standard linear solid of three elements. The validity of the model is confined to a frequency range 100 Hz–10 kHz, which was determined by the source of excitation. We have applied two validation procedures. First, the model was validated against data from another series of experiments in which the source excitation was different from the one used for estimation. A second validation test was provided by a comparison with a non-parametric identification of the complex modulus frequency by frequency [9, 16]. In both validation procedures, a good agreement was observed for both the real and the imaginary part of the complex modulus.

The model identification has been carried out both in the time and the frequency domain in order to find out possible advantages or limitations. The time domain solution was obtained by a standard finite difference method with explicit time-marching. This approach is the most general one. It is applicable for inhomogeneous media as well as nonlinear problems. The time domain solution provides direct information on different types of waves, and arrival times of waves having traveled different paths. This has been of vital importance in exploration seismology, where direct time simulations has a long history [1, 20].

On the other hand frequency domain methods offer advantages for long-range, or equivalently long-time, wave propagation problems. For example, this approach is widely used in underwater acoustics both for wave propagation and identification of sea bed parameters [10]. In the case with continuous data and models, the identification procedures in the time and the frequency domains are equivalent. However, in practice they will be based on some discretisation of both data and continuous models. The characteristics of the discrete time and frequency models are different and it may affect the outcome of the identification. We shall illustrate and discuss this point at some length in this paper.

Apart from the constitutive relationship between the normal stress and strain, lateral effects may be described with different degrees of complexity. We have made a comparison between the usual one-dimensional wave propagation model and another one based on Love's theory. The latter one involves the Poisson ratio ν for which some trial values were inserted. In the particular cases under investigation the difference between the solutions of the two models were minute.

The measurements of the present work were taken from [9]. However, a new series of experiments was also performed with the purpose to generate a nonlinear behaviour. However, despite a high-velocity axial impact with resulting strains reaching almost two percent, there was no evidence of a nonlinear wave propagation in the rod (polypropylene). Since this result does not seem to be well-known, we shall describe it in some detail.

The paper is organised as follows. In Section 2 we give a brief review of the experimental set-up. The linearity of measured strains from heavy impact loads is analysed in Section 3. Section 4 is a brief account of the time and frequency wave propagation models. The parameter estimation problem is formulated in Section 5. The finite difference method used for the time simulations is described in Section 6. The results of the optimisation are given and commented on in Sections 7 and 8. Finally, the conclusions are drawn in Section 9.

2 The experimental set-up

Wave propagation experiments were conducted at room temperature for a rod of polypropylene with density 915 kg/m^3. The bar was cylindrical with diameter 16.6 mm and had length 2000 mm. As indicated in Figure 1, the rod was impacted by a steel pendulum hammer or by a lead bullet from an air gun. The resulting strains were captured with strain gauges located at sections $x_A = 400$, $x_B = 922$, $x_C = 1354$ and $x_D = 1710$ mm respectively. The strain signals were fed from bridge amplifiers to analogue aliasing filters and finally to a digital oscilloscope. The sampling rate was 100 kHz. The experimental set-up can be studied in detail in [9].

In the estimations, the strain at x_A was used as a driving boundary condition. At the rod's free right end, the strain was put to zero. The strains at the other sections were used for least square fits and for model validations.

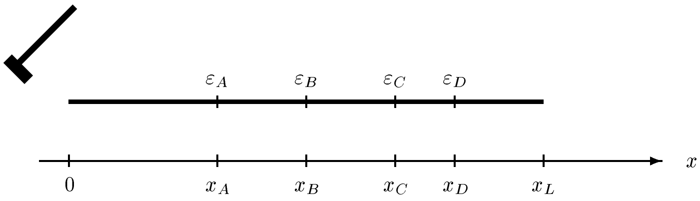

Figure 1: Schematic experimental set-up.

Finally, it should be mentioned that efforts were undertaken in order to also produce a nonlinear behaviour of the rod. An air canon were used to impact a 75 mm long steel hammer with velocities up to 50 m/s. The strength of the impact was gradually increased until the strain gauges on the rod were damaged. However, as will be treated in Section 3, no nonlinear response was found.

An example of measured strain series and their corresponding Fourier transformations at one section is given in Figure 2 for one hammer experiment and one gas canon experiment.

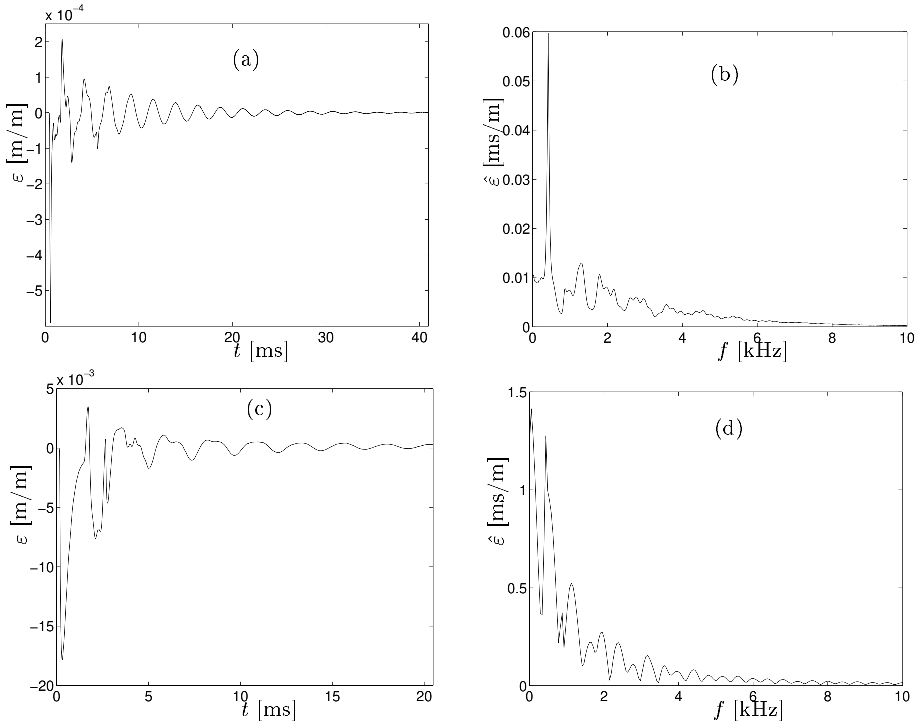

Figure 2: A measured strain serie (a) and its Fourier transformation (b) at one section for a hammer experiment. Subfigures (c) and (d) show the corresponding plots for an air canon experiment.

3 Nonlinearity in data

At an initial stage of the present study the intention was to include parameter identification of nonlinear viscoelastic models using time domain data. Therefore an attempt was made to generate a nonlinear behaviour within the same frame of experiments as in the linear case. Large strains were induced by heavy impacts at one end of the rod. In order to investigate if the measured data contained any evidence of nonlinear dynamics the following procedure was carried out.

Suppose that strains $\hat{\varepsilon}_1, \hat{\varepsilon}_2, \ldots, \hat{\varepsilon}_n$ and velocities $\hat{v}_1, \hat{v}_2, \ldots, \hat{v}_n$ at n sections are given from an experiment, where $\hat{(\cdot)}$ denotes that Fourier transformation has been undertaken. Under the assumption that data are linear, it holds, for every frequency ω_k, that

$$\begin{pmatrix} \hat{\varepsilon}_2 \\ \hat{v}_2 \end{pmatrix} = \boldsymbol{B}_1 \begin{pmatrix} \hat{\varepsilon}_1 \\ \hat{v}_1 \end{pmatrix}, \tag{1}$$

$$\begin{pmatrix} \hat{\varepsilon}_3 \\ \hat{v}_3 \end{pmatrix} = \boldsymbol{B}_2 \begin{pmatrix} \hat{\varepsilon}_2 \\ \hat{v}_2 \end{pmatrix}, \tag{2}$$

$$\vdots$$

$$\begin{pmatrix} \hat{\varepsilon}_n \\ \hat{v}_n \end{pmatrix} = \boldsymbol{B}_{n-1} \begin{pmatrix} \hat{\varepsilon}_{n-1} \\ \hat{v}_{n-1} \end{pmatrix}, \tag{3}$$

where $\boldsymbol{B}_1, \boldsymbol{B}_2, \ldots, \boldsymbol{B}_{n-1}$ are 2 by 2 matrices. By eliminating $\hat{v}_1, \hat{v}_2, \ldots, \hat{v}_n$, $n-2$ scalar relations between $\hat{\varepsilon}_1, \hat{\varepsilon}_2, \ldots, \hat{\varepsilon}_n$ are obtained as

$$\underset{(n-2,n)}{\boldsymbol{A}} \begin{pmatrix} \hat{\varepsilon}_1 \\ \vdots \\ \hat{\varepsilon}_n \end{pmatrix} = \boldsymbol{0}. \tag{4}$$

If q experiments are made, the system of equations

$$\boldsymbol{A} \begin{pmatrix} \hat{\varepsilon}_1^{(1)} & \hat{\varepsilon}_1^{(2)} & \cdots & \hat{\varepsilon}_1^{(q)} \\ \vdots & \vdots & & \vdots \\ \hat{\varepsilon}_n^{(1)} & \hat{\varepsilon}_n^{(2)} & \cdots & \hat{\varepsilon}_n^{(q)} \end{pmatrix} \triangleq \boldsymbol{A} \underset{(n,q)}{\hat{\boldsymbol{E}}} = \boldsymbol{0}, \tag{5}$$

can be formed, where the ith column contains data from the ith experiment. As $\boldsymbol{A}$ is an $(n-2) \times n$ matrix it is required that $n \geq 3$ and for the following reasoning to hold, it is further required that also $q \geq 3$. Rewrite (5) as

$$\hat{\boldsymbol{E}}^T \boldsymbol{A}^T = \boldsymbol{0}, \tag{6}$$

where $\hat{\boldsymbol{E}}^T$ is now associated with a linear transformation $\mathcal{C}^n \to \mathcal{C}^q$. Since $\boldsymbol{A}^T \neq \boldsymbol{0}$, it follows from (6) that $\hat{\boldsymbol{E}}^T$ is rank-deficient. From the size of $\boldsymbol{A}^T$ it follows that for the dimension of the null space of $\hat{\boldsymbol{E}}^T$ it holds that

$$\dim \mathcal{N}(\hat{\boldsymbol{E}}^T) \geq n-2. \tag{7}$$

Moreover, a direct sum of the null space of $\hat{\boldsymbol{E}}^T$ and the range space of $\hat{\boldsymbol{E}}$ gives

$$\mathcal{N}(\hat{\boldsymbol{E}}^T) \oplus \mathcal{R}(\hat{\boldsymbol{E}}) = \mathcal{C}^n \tag{8}$$

and from (7) and (8) it is concluded that

$$\dim \mathcal{R}(\hat{\boldsymbol{E}}) \leq 2. \tag{9}$$

To summarise, equation (9) states that the rank of the matrix $\hat{\boldsymbol{E}}$ is less than or equal to two when the assumption that data are linear holds. Since it is assumed that no further relations exist between the variables, the rank is expected to be equal to two.

An alternative is to use (44) to form

$$\hat{\boldsymbol{E}} = \begin{pmatrix} \hat{\varepsilon}_1^{(1)} & \hat{\varepsilon}_1^{(2)} & \cdots & \hat{\varepsilon}_1^{(q)} \\ \vdots & \vdots & & \vdots \\ \hat{\varepsilon}_n^{(1)} & \hat{\varepsilon}_n^{(2)} & \cdots & \hat{\varepsilon}_n^{(q)} \end{pmatrix} = \begin{pmatrix} e^{-\gamma x_1} & e^{\gamma x_1} \\ \vdots & \vdots \\ e^{-\gamma x_n} & e^{\gamma x_n} \end{pmatrix} \begin{pmatrix} \hat{P}_1 & \cdots & \hat{P}_q \\ \hat{N}_1 & \cdots & \hat{N}_q \end{pmatrix}, \tag{10}$$

that is, the columns of $\hat{\boldsymbol{E}}$ are linear combinations of the vectors $(e^{-\gamma x_i})^T$ and $(e^{\gamma x_i})^T$, $i = 1, \ldots, n$. They are linearly independent for $\gamma \neq 0$, which implies that the rank of the matrix $\hat{\boldsymbol{E}}$ is two.

In an attempt to find data with nonlinearities, $q = 17$ air gun experiments as described in Section 2 with measurements at $n = 3$ sections were carried out. The excitation in the left end of the bar specimen was increased for every experiment and the maximum absolute value of the strain in the section closest to the left end varied between 0.16 and 1.78 percent. For every frequency ω_k, the matrix $\hat{\boldsymbol{E}}$ was created and its singular values s_1, s_2, s_3 were calculated. The results are shown in Figure 3, where a logarithmic scale is used for the singular values. Introduce

$$S \triangleq \sqrt{\frac{\int s_3^2(f)\mathrm{d}f}{\int s_1^2(f)\mathrm{d}f}} \tag{11}$$

as an 'ad hoc' measure of the relation between the smallest and the largest singular values over the frequency range of interest. For the data in Figure 3, $S = 0.0068$ which indicates that it is very difficult to find any nonlinear dynamics. As a comparison, the singular values corresponding to the measurement noise are around 10^{-4}. Only linear viscoelastic theory will therefore be treated in this paper.

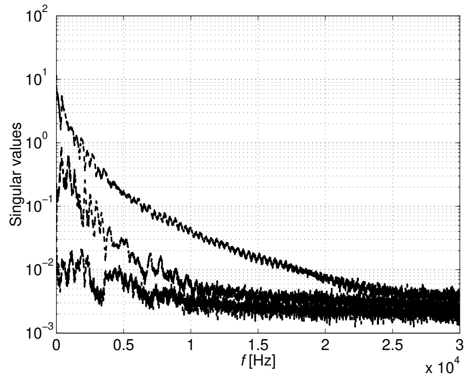

Figure 3: The singular values of the matrix $\hat{\boldsymbol{E}}$, defined in (5), for $q = 17$ experiments with measurements at $n = 3$ sections as functions of the frequency.

4 Models

4.1 Time domain models

The most basic model of one-dimensional longitudinal vibrations of a slender rod can be written

$$\rho \frac{\partial v}{\partial t} = \frac{\partial \sigma}{\partial x}, \tag{12}$$
$$\frac{\partial \varepsilon}{\partial t} = \frac{\partial v}{\partial x}, \tag{13}$$

where ρ, v, σ and ε are the density, particle velocity, stress and strain, respectively. They are assumed to be functions of one spatial coordinate x and time t only. A slight extension of the model (12)–(13) is the Love model [14]

$$\rho(1 - \nu^2 r_p^2 \frac{\partial^2}{\partial x^2}) \frac{\partial v}{\partial t} = \frac{\partial \sigma}{\partial x}, \tag{14}$$
$$\frac{\partial \varepsilon}{\partial t} = \frac{\partial v}{\partial x}, \tag{15}$$

where ν and r_p are the Poisson's ratio and the polar radius of gyration, respectively. In comparison with (12), the additional term in (14) accounts for the effect of lateral inertia. The equations (12)–(13) and (14)–(15) must be supplemented by a constitutive stress-strain relationship. We shall apply linear viscoelastic models which can be represented by a parallel array of standard linear solid models. This compound model is denoted the general standard linear solid model [4] and is shown in Figure 4. The strain ε is the same over all

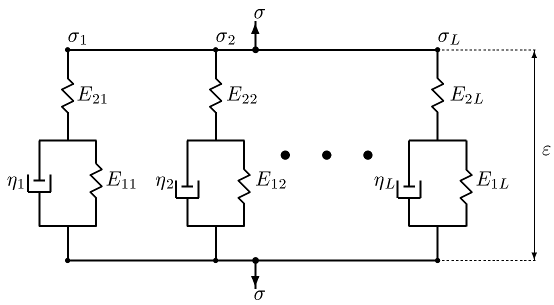

Figure 4: The general standard linear solid model, which consists of L parallel single standard linear solid models.

elements and the stress σ is

$$\sigma = \sum_{l=1}^{L} \sigma_l, \tag{16}$$

where L is the number of elements of the system. The stress-strain relationship for a single standard linear solid is

$$\sigma_l + \tau_{\sigma l}\dot{\sigma}_l = M_{Rl}(\varepsilon + \tau_{\varepsilon l}\dot{\varepsilon}), \tag{17}$$

where

$$M_{Rl} = \frac{E_{1l}E_{2l}}{E_{1l} + E_{2l}} \tag{18}$$

is the relaxed modulus and $\tau_{\sigma l}$ and $\tau_{\varepsilon l}$ are the relaxation times given by

$$\tau_{\sigma l} = \frac{\eta_l}{E_{1l} + E_{2l}}, \tag{19}$$

$$\tau_{\varepsilon l} = \frac{\eta_l}{E_{1l}}. \tag{20}$$

Following [4], we put

$$M_{Rl} = \frac{M_R}{L}. \tag{21}$$

There are $2L$ parameters $\tau_{\sigma l}$ and $\tau_{\varepsilon l}$ for $l = 1, \ldots, L$ from (19) and (20), and one parameter M_R from (18) and (21). The number of degrees of freedom of the general standard linear solid is therefore $2L + 1$.

In all there are two partial differential equations (12)–(13), or (14)–(15), for v and ε and L ordinary differential equations (17) for σ_l, $l = 1, 2, \ldots, L$, that need to be solved. Formulations based merely on v (or ε) lead to a single second order partial differential equation with a convolution operator in time, which is quite suitable to solve in the frequency domain, but awkward for time-dependent calculations. An alternative for linear models is therefore to work with frequency domain data as described in the next section.

For describing a possible nonlinear behaviour, an idea is to use nonlinear submodels in parallel with the general standard linear solid model. They would be significant only in the presence of nonlinearities. Then one or several of the equation (17) would be nonlinear. From a numerical point of view this is a minor complication because (17) is just a single equation at each spatial point.

4.2 Frequency domain models

As mentioned earlier, an alternative for the linear models is to work with frequency domain models and data. In the frequency domain, the equation of axial motion of the bar can be expressed as

$$\frac{\partial^2 \hat{\varepsilon}}{\partial x^2} - \gamma^2 \hat{\varepsilon} = 0, \tag{22}$$

where $\hat{\varepsilon}$ denotes the Fourier transform of ε and where the wave propagation coefficient $\gamma(\omega)$ and the complex modulus $E(\omega)$ are related through

$$\gamma^2(\omega) = -\frac{\rho\omega^2}{E(\omega)}. \tag{23}$$

Since the linear stress-strain relation in the frequency domain is

$$\hat{\sigma} = E(\omega)\hat{\varepsilon}, \tag{24}$$

the complex modulus for the general standard linear solid,

$$E(\omega) = \frac{M_R}{L} \sum_{l=1}^{L} \frac{1 + \mathrm{i}\omega\tau_{\varepsilon_l}}{1 + \mathrm{i}\omega\tau_{\sigma_l}}, \tag{25}$$

is given by the Fourier transformations of (16) and (17). This frequency domain model is equivalent to the time domain model described in Section 4.1, when starting with equations (12)–(13).

5 Estimation

As described in Section 4, the general standard linear solid is a constitutive stress-strain relation that models the behaviour of viscoelastic materials within the linear response area. The model consists of L parallel standard linear solid models (17). In this section the parameters in the general standard linear solid,

$$\boldsymbol{\theta} = (\tau_{\varepsilon_1}, \tau_{\sigma_1}, \ldots, \tau_{\varepsilon_L}, \tau_{\sigma_L}, M_R)^T. \tag{26}$$

are estimated using measured strains. Estimations are made with both time and frequency domain data.

5.1 Estimation using time domain data

Consider the loss function

$$J_t(\boldsymbol{\theta}) = \frac{\displaystyle\sum_{j=1}^{n}\sum_{k=1}^{N_J}\big(\varepsilon(x_j,t_k) - \varepsilon(x_j,t_k,\boldsymbol{\theta})\big)^2}{\displaystyle\sum_{j=1}^{n}\sum_{k=1}^{N_J}\varepsilon^2(x_j,t_k)}, \tag{27}$$

where $\varepsilon(x_j,t_k)$ denotes measured strain and $\varepsilon(x_j,t_k,\boldsymbol{\theta})$ denotes the strain from the time domain model at position x_j and time t_k. An estimate $\boldsymbol{\theta}_{\text{est}}$ of the unknown parameter vector $\boldsymbol{\theta}$ is obtained from (27) as

$$\boldsymbol{\theta}_{\text{est}_t} = \arg\min_{\boldsymbol{\theta}} J_t(\boldsymbol{\theta}). \tag{28}$$

The validity of the constitutive model and the quality of the estimated parameters are investigated through the validation function

$$V_t(\boldsymbol{\theta}_{\text{est}_t}) = \frac{\displaystyle\sum_{j=1}^{n}\sum_{k=1}^{N_V}\big(\varepsilon_{\text{val}}(x_j,t_k) - \varepsilon(x_j,t_k,\boldsymbol{\theta}_{\text{est}_t})\big)^2}{\displaystyle\sum_{j=1}^{n}\sum_{k=1}^{N_J}\varepsilon_{\text{val}}^2(x_j,t_k)}, \tag{29}$$

where the notation 'val' means that the data series are from another experiment and are used for validation only. Observe that the strain $\varepsilon(x_j,t_k,\boldsymbol{\theta}_{\text{est}_t})$ is calculated using boundary conditions from the validation data.

5.2 Estimation using frequency domain data

Introduce the loss function

$$J_f(\boldsymbol{\theta}) = \frac{\displaystyle\sum_{j=1}^{n}\sum_{k=1}^{N_J}\big|\hat{\varepsilon}(x_j,\omega_k) - \hat{\varepsilon}(x_j,\omega_k,\boldsymbol{\theta})\big|^2}{\displaystyle\sum_{j=1}^{n}\sum_{k=1}^{N_J}\big|\hat{\varepsilon}(x_j,\omega_k)\big|^2}, \tag{30}$$

where $\hat{\varepsilon}(x_j,\omega_k)$ denotes the Fourier transform of the measured strain and where $\hat{\varepsilon}(x_j,\omega_k,\boldsymbol{\theta})$ denotes the strain from the frequency domain model at position x_j and frequency ω_k. An estimate of $\boldsymbol{\theta}$ is obtained as

$$\boldsymbol{\theta}_{\text{est}_f} = \arg\min_{\boldsymbol{\theta}} J_f(\boldsymbol{\theta}) \tag{31}$$

and the quality of the estimated parameters is investigated through

$$V_f(\boldsymbol{\theta}_{\mathrm{est}_f}) = \frac{\displaystyle\sum_{j=1}^{n}\sum_{k=1}^{N_V}\left|\hat{\varepsilon}_{\mathrm{val}}(x_j,\omega_k) - \hat{\varepsilon}(x_j,\omega_k,\boldsymbol{\theta}_{\mathrm{est}_f})\right|^2}{\displaystyle\sum_{j=1}^{n}\sum_{k=1}^{N_V}\left|\hat{\varepsilon}_{\mathrm{val}}(x_j,\omega_k)\right|^2}. \tag{32}$$

Parseval's relation gives that the loss functions used in the time domain (27) and in the frequency domain (30) are equivalent. The same holds for the validation functions (29) and (32).

6 Calculation of model outputs

6.1 Time domain model output

In what follows the solution of the Love model (14)–(15) will be discussed. Results for the basic model (12)–(13) are simply obtained by omitting the second term in the left hand side of (14). For the solution of the equations (14)–(15) we shall apply a finite difference method with two grids that are interlaced. The first grid is defined by the grid points $x_i = x_A + i\Delta x$, $\Delta x = (x_L - x_A)/I$, $i = 0, 1, \ldots, I$ and $t_n = n\Delta t$, $n = 0, 1, \ldots, N$. A discrete representation of σ, σ_l, ε on this grid will be denoted by

$$\sigma_i^n,\ \sigma_{li}^n,\ \varepsilon_i^n, \qquad i = 0, 1, \ldots, I, \qquad l = 1, 2, \ldots, L. \tag{33}$$

The second grid is displaced half a step size both in space and time with grid points $x_{i-\frac{1}{2}} = A + (i - \frac{1}{2})\Delta x$, and $t_{n-\frac{1}{2}} = (n - \frac{1}{2})\Delta t$. The velocities

$$v_{i-\frac{1}{2}}^{n-\frac{1}{2}}, \qquad i = 1, 2, \ldots, I, \qquad n = 1, 2, \ldots, N \tag{34}$$

are accommodated on this grid, see Figure 5. The equations (14)–(15) are now approximated on the grid by the difference scheme

$$\rho(1 - \nu^2 r_p^2 D_+ D_-)\frac{1}{\Delta t}(v_{i-\frac{1}{2}}^{n+\frac{1}{2}} - v_{i-\frac{1}{2}}^{n-\frac{1}{2}}) = D_-\sigma_i^n, \qquad i = 1, 2, \ldots, I, \tag{35}$$

$$\frac{1}{\Delta t}(\varepsilon_i^{n+1} - \varepsilon_i^n) = D_- v_{i+\frac{1}{2}}^{n+\frac{1}{2}}, \qquad i = 1, 2, \ldots, I-1, \tag{36}$$

where

$$D_- u_i = \frac{1}{\Delta x}(u_i - u_{i-1}), \qquad i = 1, 2, \ldots, I, \tag{37}$$

$$D_+ u_i = \frac{1}{\Delta x}(u_{i+1} - u_i), \qquad i = 1, 2, \ldots, I. \tag{38}$$

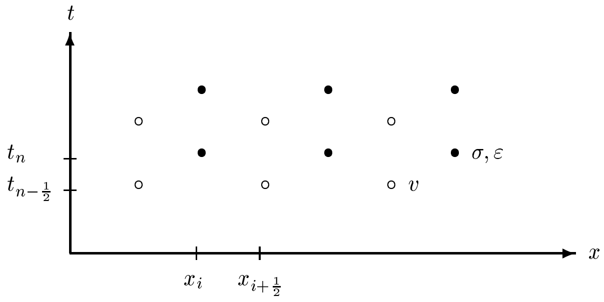

Figure 5: Location of discretised variables on a staggered grid.

For $n = 0$ and $n = -1/2$ all values are set to zero by the initial conditions. Assume that all quantities have been computed up to time levels n and $n - 1/2$. Then, for $\nu = 0$, $v_{i-\frac{1}{2}}$ for time level $n + 1/2$ can be computed from (35) using already known values. For $\nu \neq 0$, (35) defines a tridiagonal system of equations for $v_{i-\frac{1}{2}}$, $i = 1, 2, \ldots, I$, at time level $n + 1/2$. Here it should be pointed out that the boundary term

$$\frac{1}{\Delta t}(D_+ v_{N-\frac{1}{2}}^{n+\frac{1}{2}} - D_+ v_{N-\frac{1}{2}}^{n-\frac{1}{2}}) \tag{39}$$

is an approximation of

$$\frac{\partial^2 v}{\partial x \partial t} = \frac{\partial^2 \varepsilon}{\partial t^2} \tag{40}$$

at $x = x_L$, which is zero by the boundary condition $\varepsilon_L = 0$. Similarly, the corresponding term at $x = x_A$,

$$\frac{1}{\Delta t}(D_- v_{\frac{1}{2}}^{n+\frac{1}{2}} - D_- v_{\frac{1}{2}}^{n-\frac{1}{2}}) \tag{41}$$

can be evaluated from known strains at $x = x_A$.

The evaluation of the strains ε_i^{n+1} from (36) is straightforward, since this scheme is fully explicit. The boundary values ε_0^{n+1}, ε_N^{n+1} are obtained from the boundary conditions $\varepsilon_L = 0$ and $\varepsilon_A =$ measured strains.

It remains to update the stress (16) on time level $n + 1$. It is obtained by solving the ordinary differential equations (17) for the memory variables σ_l for all x_i, $i = 0, 1, \ldots, I$. First we can eliminate the time derivative of ε in (17) by letting this term be balanced by the corresponding term on the left side. The remaining part of (17) can now be solved analytically if we assume that the variation of ε_i is linear between the already computed values ε_i^n and ε_i^{n+1}. The final result of a rather lengthy calculation is

$$\begin{aligned}\sigma_{li}^{n+1} &= M_{Rl}\varepsilon_i^{n+1} + e^{-\frac{\Delta t}{\tau_{\sigma l}}}(\sigma_{li}^n - M_{Rl}\varepsilon_i^n) \\ &\quad + M_{Rl}(\frac{\tau_{\varepsilon l}}{\tau_{\sigma l}} - 1)\frac{\tau_{\sigma l}}{\Delta t}(1 - e^{-\frac{\Delta t}{\tau_{\sigma l}}})(\varepsilon_i^{n+1} - \varepsilon_i^n).\end{aligned} \tag{42}$$

It is necessary to use an implicit scheme for the solutions of equations (17) in order to avoid stability problems due to small relaxation constants $\tau_{\varepsilon l}$ and $\tau_{\sigma l}$. All variables have now been advanced to the time levels $n + 1/2$ and $n + 1$, and a new cycle can begin.

Standard von Neumann analysis [19] shows that the scheme (35)–(36) is stable if

$$\Delta t \leq \Delta x\sqrt{\frac{\rho}{E}} \tag{43}$$

for the purely elastic case $\sigma = E\varepsilon$. In fact, when the inertia term is included ($\nu > 0$), the stability condition is somewhat improved. In the viscoelastic case there is no closed formula for the stability criterion, but use of the unrelaxed modulus in the above condition seems to be sufficient [21]. It corresponds to a criterion based on the highest speed of propagation.

It is very important to compute with a sufficiently high resolution. In a one-dimensional problem like this, computer time is not a crucial factor. A suitable choice of Δx can be based on the frequency content of the input pulse at $x = 0$. For the highest frequency present, a good rule of thumb is to use 40–50 points per wavelength, which should be enough for 3–4 digits of accuracy within propagation times of 25 periods.

Staggered grids has been used for a long time in wave propagation problems in electromagnetics and elasticity [26,27]. A thorough analysis of its benefits is given in [8]. The scheme (35)–(36) is second-order accurate in the sense that the error is roughly proportional to the square of step sizes. Higher-order schemes for viscoelastic wave propagation are constructed and analysed in [21,25]. However, for problems where the influence of the boundary conditions are essential they are less flexible and more difficult to implement.

6.2 Frequency domain model output

The analytical solution to Equation (22) is

$$\hat{\varepsilon} = \hat{P}e^{-\gamma x} + \hat{N}e^{\gamma x}, \tag{44}$$

where $\hat{P}$ and $\hat{N}$ are determined from two boundary conditions. As in Section 6.1, use is made of the boundary condition $\hat{\varepsilon}_L = 0$ and the measured strains at $x = x_A$.

7 Results

To begin with, a comparative study of the basic model (12)–(13) and the Love model (14)–(15) was made for a representative set of material parameters. The time calculations were driven by measured strain values at section x_A, see Figure 1. We found that the difference between the solutions of the two models was quite small (<0.1 percent). Therefore the Love model was ignored in the subsequent investigation. This confirms the results of Section 3, since it seems to be possible to describe data with a linear wave propagation model.

The optimisations (28) and (31) in the time and in the frequency domain were based on solutions to the basic model (12)–(13). In the frequency domain there is an analytic solution (44) which can be evaluated almost exactly. The time domain solution was obtained by the finite difference method described in Section 6.1. The numerical error of the solution decreases by the squares of the stepsizes Δt and Δx used for the approximation of the wave equation. We have chosen to compute with stepsizes so small that the discretisation error can be regarded as negligible (<0.1 percent). The implementation was made in Fortran 77.

The optimisations (28) and (31) were performed by the MATLAB® optimization toolbox routine 'fminsearch' [5] which uses the simplex search method of [11]. Initial values of the parameters for the estimation were taken from the constant Q model, where $Q = \mathrm{Re}\{E(\omega)\}/\mathrm{Im}\{E(\omega)\}$ is the quality factor. The constant Q model and its algorithm are described in [4].

One important question is how many single standard linear solid models the compound model should contain. The values of the loss functions (27) and (30) decrease when the number of submodels L increase. This is so because the parametric fit to the estimation data will always be better with a larger model order. It is therefore advantageous to validate the models on a fresh data set that has not been used in the estimation, as is done in (29) and (32), see [13,22].

The optimal value of the loss function (27) and the corresponding value of the validation function (29) in the time domain with $n = 3$ and $N_J = N_V = 4096$ are compared in Table 1 for different number of submodels L.

L	$J_t(\boldsymbol{\theta}_{\mathrm{est}_t}) \cdot 10^3$	$V_t(\boldsymbol{\theta}_{\mathrm{est}_t}) \cdot 10^3$
1	49.53	44.55
2	12.08	7.20
3	7.82	6.19

Table 1: The loss function $J_t(\boldsymbol{\theta}_{\mathrm{est}_t})$ and the validation function $V_t(\boldsymbol{\theta}_{\mathrm{est}_t})$, defined in (27) and (29), with $n = 3$ and $N_J = N_V = 4096$ for different number of submodels L.

The corresponding results for the loss and validation functions (30) and (32) in the frequency domain are given in Table 2. From Table 2 it is seen that the validation function $V_f(\boldsymbol{\theta}_{\text{est}_f})$ has a minimum for $L = 3$. Therefore only the case of three submodels will be considered in the following.

L	$J_f(\boldsymbol{\theta}_{\text{est}_f}) \cdot 10^3$	$V_f(\boldsymbol{\theta}_{\text{est}_f}) \cdot 10^3$
1	32.03	29.75
2	5.84	4.24
3	4.75	3.57
4	4.70	3.58

Table 2: The loss function $J_f(\boldsymbol{\theta}_{\text{est}_f})$ and the validation function $V_f(\boldsymbol{\theta}_{\text{est}_f})$, defined in (30) and (32), with $n = 3$ and $N_J = N_V = 4096$ for different number of submodels L.

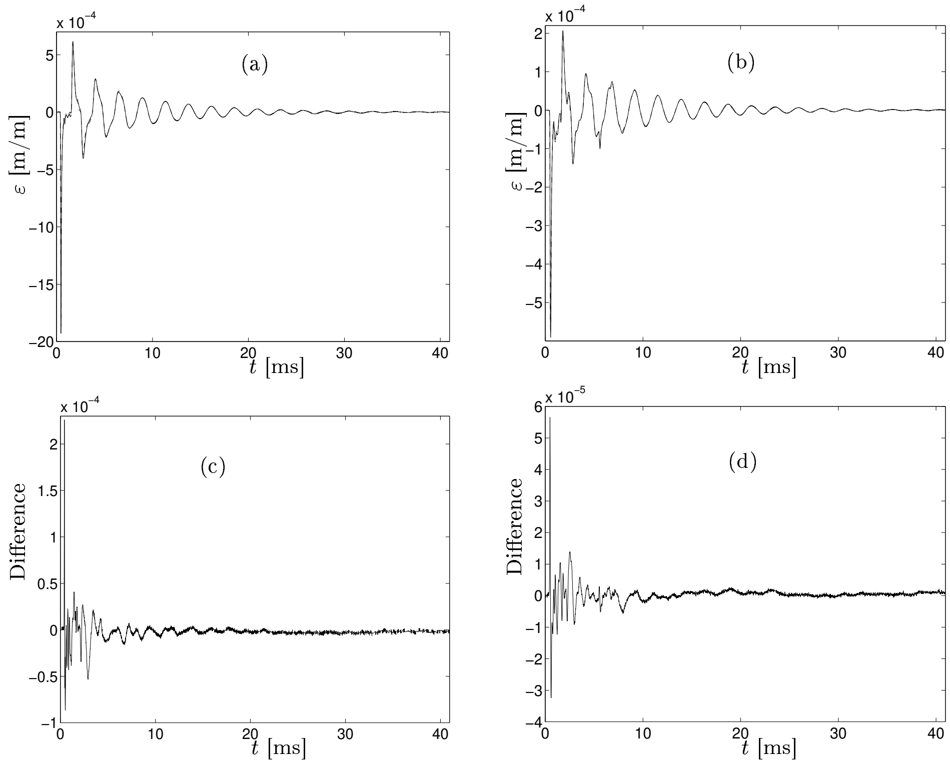

Figure 6: The measured strain $(--)$ in x_B and the calculated strain $(-)$ based on the estimated parameter vector $\boldsymbol{\theta}_{\text{est}_t}$ for $L = 3$, $n = 3$, $N_J = 4096$ and the basic model in section x_B. Results for estimation (from air gun experiment) and validation (from hammer experiment) data are shown in (a) and (b), respectively. The differences between the measured and calculated strains are shown in (c) and (d).

Two model structure selection criteria were also used, Akaike's information criteria (AIC) and the final prediction error criterion (FPE), see [13, 22] and the references therein. Both criteria gave larger model orders than the ones considered here. However, in [22] it is shown that the AIC and FPE do not give consistent estimates of the model order. The risk of overfitting is 15.7 percent, even for a large number of data points. Considering that risk and that it for practical reasons is undesirable to have a too high model order, the results from Table 2 motivates the choice of $L = 3$ submodels.

Figure 6 shows a graph of the time domain solution with $\boldsymbol{\theta}_{\mathrm{est}_t}$ and measured strain at section x_B. As can be seen there is a close agreement between the curves. The corresponding curves in the frequency domain are shown in Figure 7. Note that the computational burden for the time domain approach is much higher than for the frequency domain approach. This is so because the time domain model output is based on a numerical solution to a partial differential equation whereas the frequency domain model output is obtained from an analytical solution to an ordinary differential equation.

8 Discussions

There is a discrepancy between the results of Tables 1 and 2 despite that the norms are entirely equivalent according to Parseval's relation. For $L = 3$ there are seven free parameters in (26) of the compound model. The optimal values $\boldsymbol{\theta}_{\mathrm{est}_t}$ and $\boldsymbol{\theta}_{\mathrm{est}_f}$ are shown in Table 3. As a consequence of the difference in

	$\boldsymbol{\theta}_{\mathrm{est}_t}$	$\boldsymbol{\theta}_{\mathrm{est}_f}$
τ_{ε_1} [ms]	$2.30 \cdot 10^{-3}$	$5.57 \cdot 10^{-4}$
τ_{σ_1} [ms]	$1.13 \cdot 10^{-3}$	$3.90 \cdot 10^{-4}$
τ_{ε_2} [ms]	$9.20 \cdot 10^{-5}$	$7.05 \cdot 10^{-5}$
τ_{σ_2} [ms]	$5.51 \cdot 10^{-5}$	$4.56 \cdot 10^{-5}$
τ_{ε_3} [ms]	$6.94 \cdot 10^{-6}$	$1.43 \cdot 10^{-5}$
τ_{σ_3} [ms]	$9.93 \cdot 10^{-7}$	$8.59 \cdot 10^{-6}$
M_R [GPa]	$1.94 \cdot 10^{9}$	$2.36 \cdot 10^{9}$

Table 3: The result of the optimisation (28) and (31) for $L = 3$.

estimated parameter vectors the corresponding complex moduli will not coincide. This is seen in Figure 8, where the result of a comparison between the complex moduli obtained from the parametric estimates (27) and (30) for $L = 3$ and the complex modulus from the non-parametric frequency domain estimate in [9, 16] is shown. The discrepancy in $\mathrm{Re}\{E(\omega)\}$ is substantial for higher frequencies as can be seen from Figure 8. In an attempt to analyse this difference, the solutions were recomputed in both the time and frequency domain using an exchange of

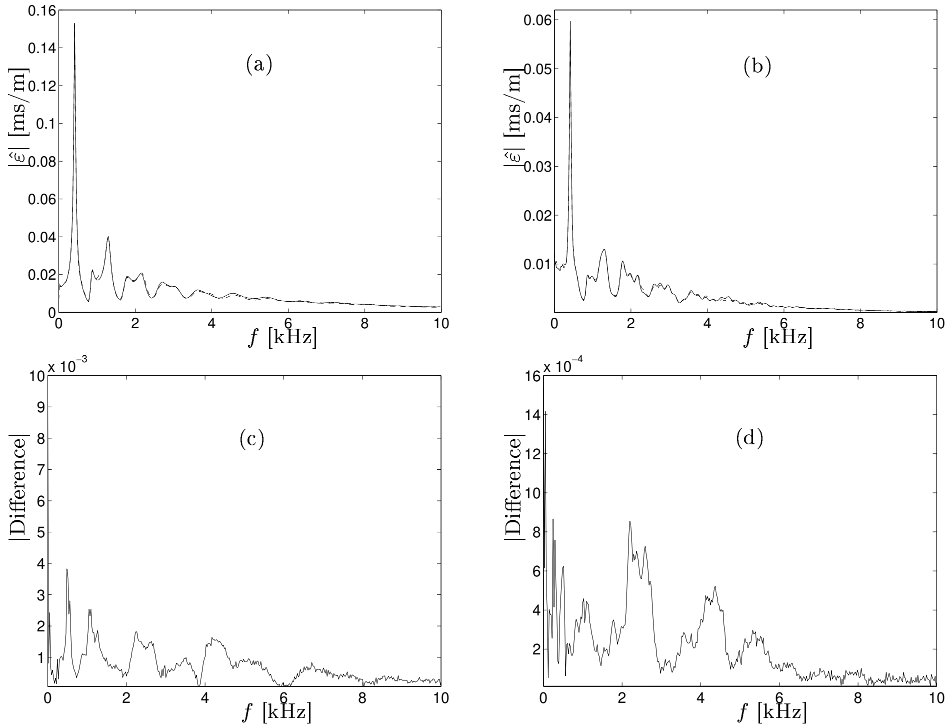

Figure 7: The absolute values of the Fourier transformed measured strain $(--)$ in x_B and the calculated strain (–) based on the estimated parameter vector $\boldsymbol{\theta}_{\mathrm{est}_f}$ for $L = 3$, $n = 3$, $N_J = 4096$ and the basic model in section x_B. Results for estimation (from air gun experiment) and validation (from hammer experiment) data are shown in (a) and (b), respectively. The absolute values of the differences between the measured and calculated strains are shown in (c) and (d).

the optimal parameters $\boldsymbol{\theta}_{\mathrm{est}_t}$ and $\boldsymbol{\theta}_{\mathrm{est}_f}$. There was no improvement of the loss functions, although the differences $V_t(\boldsymbol{\theta}_{\mathrm{est}_t}) - V_t(\boldsymbol{\theta}_{\mathrm{est}_f})$ and $V_f(\boldsymbol{\theta}_{\mathrm{est}_f}) - V_f(\boldsymbol{\theta}_{\mathrm{est}_t})$ turned out to be quite small. Hence, it is not a reasonable explanation of the differences between $\boldsymbol{\theta}_{\mathrm{est}_t}$ and $\boldsymbol{\theta}_{\mathrm{est}_f}$ that the optimisation algorithm stopped in a local minima.

The uncertainty in the determination of $\mathrm{Re}\{E(\omega)\}$ in the time domain is surprisingly large in view of the good fit as displayed in Figure 6. One possible explanation is that the attenuation of higher frequencies are relatively large and their phase velocities, which are closely related to $\mathrm{Re}\{E(\omega)\}$, are of less importance. Yet, the same reasoning could be applied to the frequency domain solution.

However, there is a fundamental difference in the treatment of the driving at x_A, see Figure 1. The input at x_A consists of data of measured strains. They

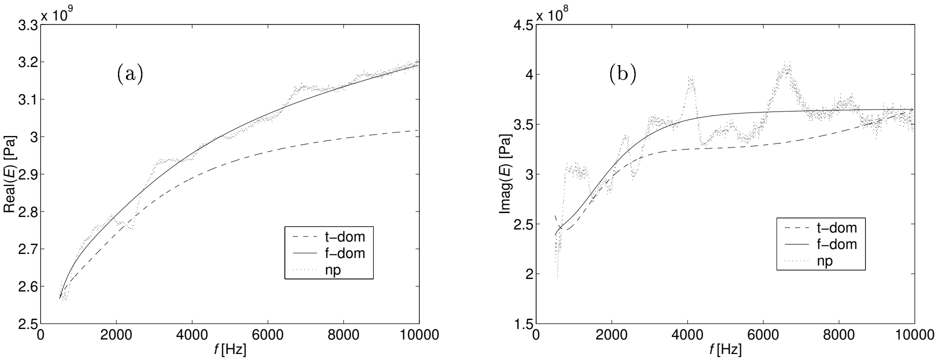

Figure 8: The complex modulus given by the general standard linear solid model (25) where the parameters are obtained from estimations using time domain data ($--$) and frequency domain data ($-$) at $n = 3$ sections with $N_J = 4096$ for $L = 3$ parallel standard linear solid models. The complex modulus given by the non-parametric identification in [9] ($\cdots$), also shown in Figure 4 (c) of [9]. The results for the real part and imaginary part are shown in (a) and (b), respectively, as functions of frequency.

are sampled with a timestep $\Delta t_s = 10^{-5}$ s. The time-discrete boundary data are identical for both approaches. The time domain model is implemented by the finite difference method with stepsizes Δt and Δx. To obtain high accuracy of the discrete transmission model, it is necessary to compute with $\Delta t < \Delta t_s$. It implies that the discrete time points of the boundary data do not coincide with those of the finite difference solver. Therefore linear interpolation of the boundary data is applied in the present implementation. In the limit $\Delta t \to 0$ and $\Delta x \to 0$, it corresponds to a continuous driving function at the boundary which is piecewise linear between measured values. The frequency domain solution is based on discrete Fourier transformation of the data at x_A. It implies that a time window $[0, T]$ is introduced and the fast Fourier transform is applied to all points within the window. The continuous counterpart in the time domain is a finite Fourier series with the period T which interpolates the given points. The window must be chosen large enough in order to avoid Gibbs' phenomenon. Otherwise the trigonometric interpolant will be oscillatory, although it goes through the sampling points. In conclusion, the driving at the boundary, viewed as a continuous function, is distinct for the two approaches. In the time domain model it is represented by a piecewise linear polynomial through the data points. In the frequency domain the driving can be interpreted as an interpolating trigonometric polynomial.

To reconcile the results of Table 3 and Figure 8 we have recomputed the optimisation in the time domain with a treatment of boundary data that better resembles that for the frequency domain model. Namely, the density of boundary data was doubled by inserting new values at the midpoints of the original sampling points. The new values were obtained by trigonometric interpolation. Technically this is most conveniently accomplished by appending zeros to the original Fourier transform so that its size is doubled. The inverse transform to the time domain now provides the desired values. The results from the new optimisation in the time domain for $L = 3$ are shown in Tables 4 and 5 and in Figure 9. For reference, the frequency domain results have also been included in Table 5 and in Figure 9, although they are the same as before. As can be noticed from Figures 8 and 9, there is now a better agreement between the time and the frequency results.

L	$J_t(\boldsymbol{\theta}_{\text{est}_t}) \cdot 10^3$	$V_t(\boldsymbol{\theta}_{\text{est}_t}) \cdot 10^3$
1	38.95	36.42
2	7.33	5.13
3	5.10	3.97

Table 4: The loss function $J_t(\boldsymbol{\theta}_{\text{est}_t})$ and the validation function $V_t(\boldsymbol{\theta}_{\text{est}_t})$, defined in (27) and (29), with $n = 3$ and $N_J = N_V = 4096$ for different number of submodels L. The boundary data were obtained by trigonometric interpolation.

	$\boldsymbol{\theta}_{\text{est}_t}$	$\boldsymbol{\theta}_{\text{est}_f}$
τ_{ε_1} [ms]	$8.07 \cdot 10^{-4}$	$5.57 \cdot 10^{-4}$
τ_{σ_1} [ms]	$5.30 \cdot 10^{-4}$	$3.90 \cdot 10^{-4}$
τ_{ε_2} [ms]	$7.34 \cdot 10^{-5}$	$7.05 \cdot 10^{-5}$
τ_{σ_2} [ms]	$4.60 \cdot 10^{-5}$	$4.56 \cdot 10^{-5}$
τ_{ε_3} [ms]	$8.47 \cdot 10^{-6}$	$1.43 \cdot 10^{-5}$
τ_{σ_3} [ms]	$3.78 \cdot 10^{-6}$	$8.59 \cdot 10^{-6}$
M_R [GPa]	$2.26 \cdot 10^{9}$	$2.36 \cdot 10^{9}$

Table 5: The result of the optimisation (28) and (31) for $L = 3$. The boundary data for the time domain problem were obtained by trigonometric interpolation.

In a further attempt to analyse the difference in the estimates, a vector $\boldsymbol{\theta}$ for $L = 3$ was chosen and the time domain and frequency domain model outputs were calculated. The time domain model output was Fourier transformed and compared with the frequency domain model output through

$$r \triangleq \frac{\sum_{j=1}^{n} \sum_{k=1}^{N_J} \left| \hat{\varepsilon}(x_j, \omega_k, \boldsymbol{\theta}) - \mathcal{F}\{\varepsilon(x_j, t_k, \boldsymbol{\theta})\} \right|^2}{\sum_{j=1}^{n} \sum_{k=1}^{N_J} \left| \hat{\varepsilon}(x_j, \omega_k, \boldsymbol{\theta}) \right|^2} \approx 3.03 \cdot 10^{-3}, \tag{45}$$

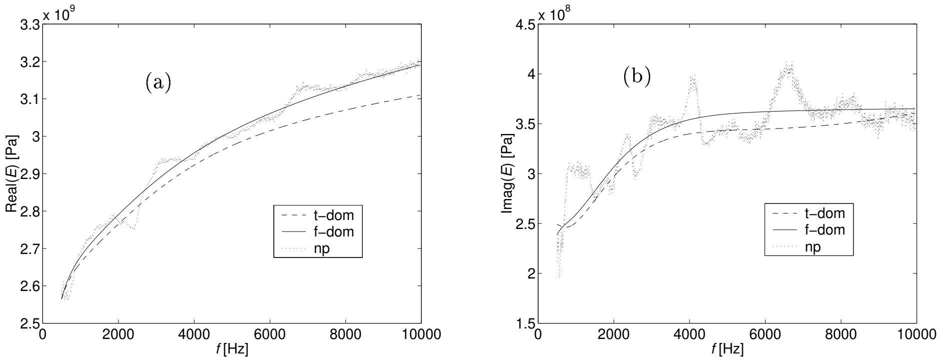

Figure 9: The complex modulus given by the general standard linear solid model (25) where the parameters are obtained from estimations using time domain data (−−) and frequency domain data (–) at $n = 3$ sections with $N_J = 4096$ for $L = 3$ parallel standard linear solid models. The complex modulus given by the non-parametric identification in [9] with $(\cdots)$, also shown in Figure 4(c) of [9]. The results for the real part and imaginary part are shown in (a) and (b), respectively, as functions of frequency. The boundary data for the time domain problem were obtained by trigonometric interpolation.

where $n = 3$, $N_J = 4096$ and where $\hat{\varepsilon}(x_j, \omega_k, \boldsymbol{\theta})$ is the frequency domain model output, $\varepsilon(x_j, t_k, \boldsymbol{\theta})$ is the time domain model output and $\mathcal{F}$ denotes discrete Fourier transformation. The time and frequency domain estimates for $L = 3$ are denoted $\boldsymbol{\theta}_{\mathrm{est}_t}$ and $\boldsymbol{\theta}_{\mathrm{est}_f}$, respectively. Then, for the validation functions (29) and (32), it holds that $V_t(\boldsymbol{\theta}_{\mathrm{est}_f}) - V_t(\boldsymbol{\theta}_{\mathrm{est}_t}) \approx 3.07 \cdot 10^{-3}$ and $V_f(\boldsymbol{\theta}_{\mathrm{est}_f}) - V_f(\boldsymbol{\theta}_{\mathrm{est}_t}) \approx 5.82 \cdot 10^{-4}$. Given the value of the error r in (45), these differences may be acceptable.

It is desirable that the time window of the frequency domain approach is so wide that the signal strength has decayed to zero at its end. This condition is fairly well fulfilled in the present case. To illustrate the detrimental effect of a too small time window, the data series of the optimisation scheme was truncated already at 256 samples instead of 4096. The results of the optimisation with the short time series is shown in Figure 10. Obviously the time domain approach suffers less from a small window. This indicates that estimation with time domain data is preferable when only short data series are available.

9 Conclusions

This study shows that it is possible to derive a general standard linear solid model of the elasticity modulus of a viscoelastic material (polypropylene) by the use of measured strains from wave propagation experiments. The model parameters (relaxation times) were identified by minimisation of the difference between

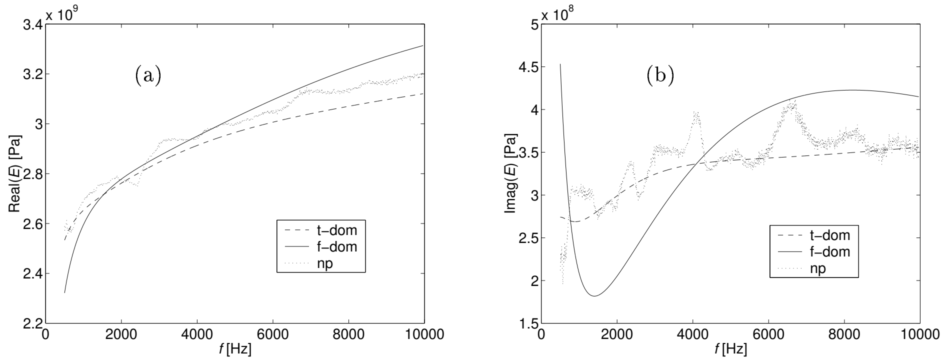

Figure 10: The complex modulus given by the general standard linear solid model (25) where the parameters are obtained from estimations using time domain data (−−) and frequency domain data (–) at $n = 3$ sections for $L = 3$ parallel standard linear solid models. In this case, $N_J = 256$. The complex modulus given by the non-parametric identification in [9] with $(\cdots)$. The results for the real part and imaginary part are shown in (a) and (b), respectively, as functions of frequency. The boundary data for the time domain problem were obtained by trigonometric interpolation.

measured and model computed strains. Only a few parameters were needed to reproduce the viscoelastic behaviour with good accuracy in the frequency range 100 Hz–10 kHz of the the available data.

The pros and cons of system identification in the time and frequency domain have been illustrated. In the present case the frequency domain approach is preferable. The model output in the frequency domain is obtained from an analytical solution which makes this approach fast. However its performance deteriorates if the time window is too small. The time domain approach is local in time and the optimisation is less sensitive to the length of the time integration. However we have observed that a good fit of time domain data does not necessarily imply the same for the elasticity module. A similar observation was made in [23] and further studies are needed to clarify this point. Another topic for further investigations is the influence on the parameter identification of the discretisation errors of the finite difference method.

Acknowledgment

The authors are grateful to Eva Mossberg for programming help and to Prof. Torsten Söderström for discussions and comments on the manuscript and to Prof. Bengt Lundberg for discussions.

References

[1] Z. Alterman and F. C. Karal Jr. Propagation of elastic waves in layered media by finite-difference methods. *Bull. Seism. Soc. Am.*, 58:367–398, 1968.

[2] J. L. Buchanan. Numerical solution for the dynamic moduli of a viscoelastic bar. *J. Acoust. Soc. Am.*, 81(6):1775–1786, June 1987.

[3] J. M. Carcione, D. Kosloff, and R. Kosloff. Wave propagation simulation in a linear viscoelastic medium. *Geophys. J. R.*, 95:597–611, 1988.

[4] G. Casula and J. M. Carcione. Generalized mechanical model analogies of linear viscoelastic behaviour. *Bollettino Di Geofisica Teorica Ed Applicata*, 34(136):235–256, December 1992.

[5] T. Coleman, M. A. Branch, and A. Grace. *Optimization Toolbox. For Use with MATLAB®*. The MathWorks, Inc., Natick, MA, USA, January 1999. Third printing revised for version 2 (release 11).

[6] S. M. Day and J. B. Minster. Numerical simulation of attenuated wavefields using a Pade approximant method. *Geophys. J. Roy. Astr. Soc.*, 78:105–118, 1984.

[7] H. Emmerich and M. Korn. Incorporation of attenuation into time-domain computations of seismic waves fields. *Geophysics*, 52:1252–1264, 1987.

[8] B. Fornberg. High-order finite differences and the pseudospectral method on staggered grids. *SIAM J. Numer. Anal.*, 27:904–918, 1990.

[9] L. Hillström, M. Mossberg, and B. Lundberg. Identification of complex modulus from measured strains on an axially impacted bar using least squares. *Journal of Sound and Vibration*, 230(3):689–707, February 2000.

[10] F. B. Jensen, W. A. Kuperman, M. B. Porter, and H. Schmidt. *Computational Ocean Acoustics*. AIP Press, New York, 1994.

[11] J. C. Lagarias, J. A. Reeds, M. H. Wright, and P. E. Wright. Convergence properties of the nelder-mead simplex method in low dimensions. *SIAM Journal on Optimization*, 9(1):112–147, 1998.

[12] R. S. Lakes. *Viscoelastic Solids*. CRC Press, 1999.

[13] L. Ljung. *System Identification*. Prentice–Hall, Upper Saddle River, NJ, USA, 2nd edition, 1999.

[14] A. E. H. Love. *The Mathematical Theory of Elasticity*. Cambridge University Press, fourth edition, 1927. Section 278.

[15] B. Lundberg and R. H. Blanc. Determination of mechanical material properties from the two-point response of an impacted linearly viscoelastic rod specimen. *Journal of Sound and Vibration*, 126(1):97–108, 1988.

[16] M. Mossberg, L. Hillström, and T. Söderström. Non-parametric identification of viscoelastic materials from wave propagation experiments. Submitted to *Automatica*.

[17] S. Ödeen and B. Lundberg. Determination of complex modulus from measured end-point accelerations of an impacted rod specimen. *Journal of Sound and Vibration*, 165(1):1–8, 1993.

[18] L. Peirlinckx, R. Pintelon, and L. Van Biesen. Identification of parametric models for ultrasonic wave propagation in the presence of absorption and dispersion. *IEEE Trans. on Ultrasonics, Ferroelectrics, and Frequency Control*, 40(4):302–312, July 1993.

[19] R. D. Richtmyer and K. W. Morton. *Difference Methods for Initial-Value Problems.* Wiley, New York, 2nd edition, 1967.

[20] N. H. Ricker. *Transient Waves in Visco-Elastic Media.* Elsevier, Amsterdam, 1977.

[21] J. O. A. Robertsson, J. O. Blanch, and W. W. Symes. Viscoelastic finite-difference modeling. *Geophysics*, 99:1444–1456, 1994.

[22] T. Söderström and P. Stoica. *System Identification.* Prentice–Hall International, Hemel Hempstead, United Kingdom, 1989.

[23] Y. Sogabe and M. Tsuzuki. Identification of the dynamic properties of linear viscoelastic materials by the wave propagation testing. *Bulletin of the Japan Society of Mechanical Engineers*, 29(254):2410–2417, August 1986.

[24] M. Soula, T. Vinh, Y. Chevalier, T. Beda, and C. Esteoule. Measurements of isothermal complex moduli of viscoelastic materials over a large range of frequencies. *Journal of Sound and Vibration*, 205(2):167–184, 1997.

[25] H. Tal-Ezer, J. M. Carcione, and D. Kosloff. An accurate and efficient scheme for wave propagation in linear viscoelastic media. *Geophysics*, 55:1366–1379, 1990.

[26] J. Virieux. P-SV wave propagation in heterogeneous media: Velocity-stress finite difference method. *Geophysics*, 51:889–901, 1986.

[27] K. S. Yee. Numerical solution of initial boundary value problems: Maxwell's equations in isotropic media. *IEEE Trans. Antennas Propagat.*, AP–14:302–307, 1966.